

Coastal-Trapped Waves behind a Large Continental Shelf Island, Southern Great Barrier Reef

DAVID A. GRIFFIN AND JASON H. MIDDLETON

Faculty of Science, University of New South Wales, Kensington, N.S.W. 2033, Australia

(Manuscript received 12 November 1985, in final form 24 March 1986)

ABSTRACT

The salient features of subinertial frequency fluctuations of current, sea level, temperature and wind stress observed within the Capricornia section of the Great Barrier Reef are interpreted by comparison with coastal-trapped wave (CTW) theories. Near-coastal currents and sea levels are modeled with some success by a theory of first-mode wind-forced barotropic continental shelf waves with geographical origin at Fraser Island, the southern across-shelf boundary of the study region. However, current and temperature variations of period 8–10 days on the continental slope are observed to have energy far in excess of that generated by the local wind. Decomposition of the observed alongshore velocity field in terms of baroclinic CTW modes indicates the signal is predominantly a second- or third-mode wave propagating equatorward at $0.4\text{--}0.6\text{ m s}^{-1}$. These modes have most of their energy flux propagating along the continental slope, and the energy levels indicate that the source region lies to the south of Fraser Island. The possible biological and geological relevance of CTW activity within the study region is briefly discussed.

1. Introduction

The east coast of Australia is the region where continental shelf waves were first discovered (Hamon, 1962, 1966). Since then there have been many observations and theoretical models describing the broader class of coastal-trapped waves (CTWs). (e.g., See the reviews by Allen, 1980; Mysak, 1980a,b.) The present work concerns measurements made on the east coast of Australia in a region located at the most southerly extent of the Great Barrier Reef (GBR). The experiment was designed to test the theory of wind-driven continental shelf waves from a geographical origin (Middleton and Cunningham, 1984) using Fraser Island (FI) as the southern boundary of the study region. Another impetus for a general shelf-circulation study of this region of the GBR came as a result of the declaration of the region as the first section of the GBR Marine Park. In addition, as far as logistics allowed, instrument deployment was scheduled to overlap in time with the extensive Australian Coastal Experiment (ACE; Freeland et al., 1986; Church et al., 1986a,b) farther south.

The continental shelf of the southern part of the GBR has a complex geographical structure with FI at 25°S extending from the coast to within 3 km of the shelf break (Fig. 1). South of FI the continental shelf is narrow (30–50 km), only slowly varying in the alongshore direction, and adjacent to an ocean of depth 4400 m. North of FI coral cays and reefs occupy the outer edge of a relatively flat shelf of width ~ 65 km, which drops away to the Marion Plateau of only ~ 440

m depth. This drop will hereafter be referred to as the continental slope although it does not strictly deserve the title. At 200 km northwest of FI the shelf widens abruptly at the Capricorn Channel to a width of over 200 km. Studies of continental shelf waves north of the Capricorn Channel have been made by Middleton (1983) and Middleton and Cunningham (1984) but no previous current measurements except the drifter studies of Woodhead (1970) have been made between FI and the Capricorn Channel.

Despite the general topographic complexity, current meters and pressure gauges were placed north of FI at locations deemed suitable for a comparison of recorded data with wind-driven continental shelf wave theories. An unexpected result is that little of the observed variability in the subinertial frequency currents is locally wind driven. Instead, it appears that the low-frequency spectrum is dominated by fluctuations that have propagated from regions south of FI. Significant energy has therefore found its way past the obstruction comprised of FI and its associated reef named Breaksea Spit, in contrast to the predictions for ACE of Clarke and Thompson (1984) and the early observations of Hamon (1966).

This paper is organized as follows. Section 2 outlines the field program and the observations, while section 3 compares the predictions of a barotropic wind-driven shelf wave theory with the wind-driven response on the continental shelf within the study region. In section 4 the relation between our data and data collected simultaneously for ACE at Evans Head (440 km south of FI) is studied to determine the source of the vari-

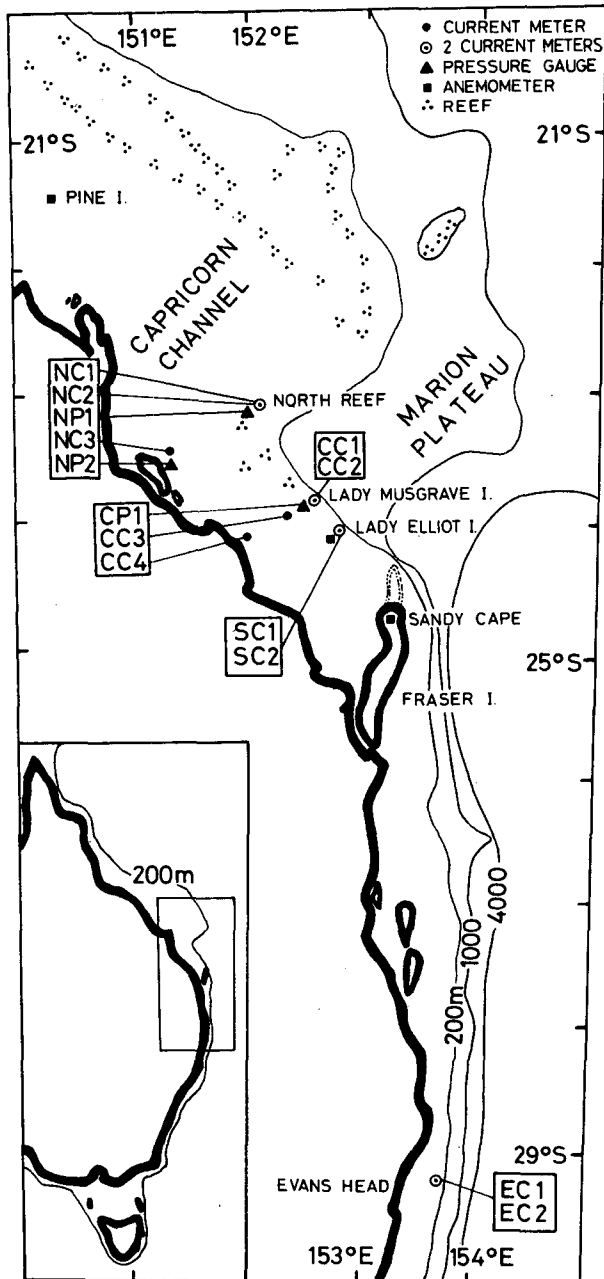


FIG. 1. Map of eastern Australia showing the locations of recording instruments. See Table 1 for further information.

ability observed on the upper continental slope in the study region north of FI. Possible baroclinic free CTW modal structures are computed for the continental shelf topography north of FI, and in section 5 these are discussed with reference to the observed propagation of waves through the study region. Section 6 concludes with a summary and discussion.

2. The field program and the observations

In June 1983 six current meter moorings and four pressure gauges were deployed in the study region from

the CSIRO RV *Sprightly*. Six months later these were retrieved using the charter boat *Sea Mare*. Three current meter moorings, equipped with two current meters each, were deployed near the shelf break, and the remaining three moorings were placed on the shelf proper with one current meter per mooring. Pressure gauges were deployed using SCUBA in less than 10 m of water on the outer edges of reefs. The locations of the three successfully retrieved pressure gauges and of the six current meter moorings are depicted in Fig. 1, which also shows the locations of stations recording meteorological data that was later acquired from the Bureau of Meteorology. The instruments used were Aanderaa RCM4s and WLR5s, these being set to sample once an hour. Instrument depths and codes are listed in Table 1.

All current meters were deployed far enough away from reefs to ensure that local topographic effects did not bias the measurements and deep enough so that swell-induced rotor run-up was not a problem (Pierson et al., 1981). To remove tidal and inertial period (29.4 h) motions, calibrated hourly values of current and pressure data were low-pass filtered using a Fourier transform filter (Walters and Heston, 1982), which sets to zero the Fourier coefficients corresponding to periods less than 40 h before retransforming. The filter is cosine-tapered in the region of the cutoff frequency to minimize the Gibbs phenomenon. The number of hourly

TABLE 1. Instrument depths and codes. The first letter, N, C, S or E, stands for northern, central, southern and Evans Head, respectively. The second letter, C or P, indicates current meters or pressure gauges, respectively. Numbering on each line starts at the deepest, most seaward instrument. The water depth listed for pressure gauges is the mean depth surrounding the reef on which the gauges were deployed.

Instrument line	Bottom depth (m)	Instrument depth (m)	Code
Northern			
North Reef to Cape	62	55	NC1
Capricorn	62	45	NC2
	55	5	NP1
	32	25	NC3
	14	2	NP2
Central			
Lady Musgrave Island to Round Hill	160	130	CC1
Head	160	70	CC2
	50	9	CP1
	40	33	CC3
	30	23	CC4
Southern			
Lady Elliot Island	160	130	SC1
	160	70	SC2
Evans Head			
	200	190	EC1
—	200	125	EC2

records used were reduced until the total had prime factors less than 97 before the series was transformed (Brenner, 1967). This procedure minimizes the data loss that can occur with less prime factors. The filtered data were then subsampled to daily (noon) values for subsequent analysis.

The meteorological data were provided as 0900 and 1500 LST readings, and these were vector-averaged to yield a noon value. The resultant data from two nearby meteorological stations (Sandy Cape and Lady Elliot Island) were then averaged in the frequency domain to yield a single wind-velocity time series. Wind stress was then calculated using a continuous function derived by Wu (1982).

The resulting daily dataset is plotted in Fig. 2 which, for the vector quantities wind stress and current, are portrayed in the form of vector stick diagrams oriented so that the local alongshore component points directly up the page. Bottom-mounted pressure gauges record the total pressure, which is the quantity of dynamic importance, so atmospheric pressure changes need not

be taken into account. For display purposes, however, the scale is calibrated in centimeters of water. Inspection of Fig. 2 suggests that three distinct time subintervals exist, which are distinguished from each other by (i) direction of mean current, (ii) degree of baroclinicity, and (iii) amount of energy in the 6–10 day period band. The three time subintervals are compared in section 3 and for practical reasons they are assigned equal lengths of 53 days.

Cartesian spectra, in energy-preserving form, of the detrended time series are shown in Fig. 3. The most energetic motions within the study region are at periods of approximately 10 days on the continental slope near FI rather than on the shelf proper. This suggests that further analysis is likely to reveal that these motions are not locally wind-driven, as is discussed in section 3.

As input to wind-driven circulation models we will require estimates of the wavenumber of the wind stress. Cross-spectral estimates of alongshore wind stress evaluated from the meteorological stations at Sandy

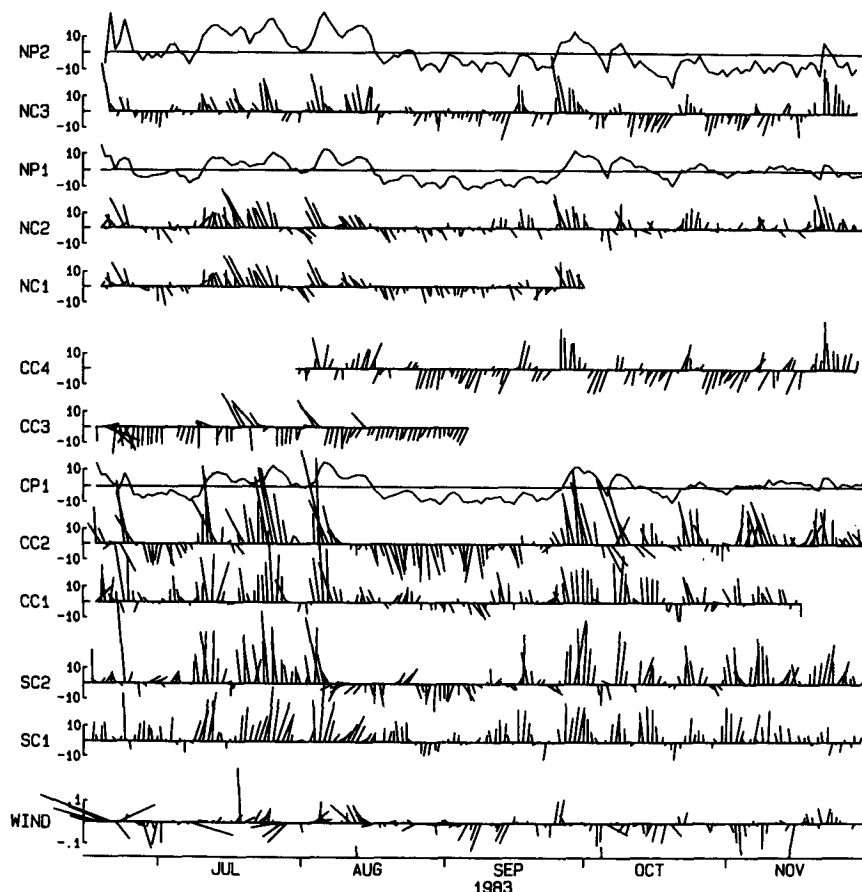


FIG. 2. The dataset from instruments within the study region. All time series have been low passed at the 40 h period and subsampled at daily intervals. Current vectors pointing straight up the page are oriented directly alongshore. Velocity is in cm s^{-1} . The pressure gauge data are total pressure expressed in cm of seawater. Wind stress is the frequency-domain average of two nearby stations and is plotted in N m^{-2} . The vertical ticks on the time axis indicate the three time segments discussed in section 3.

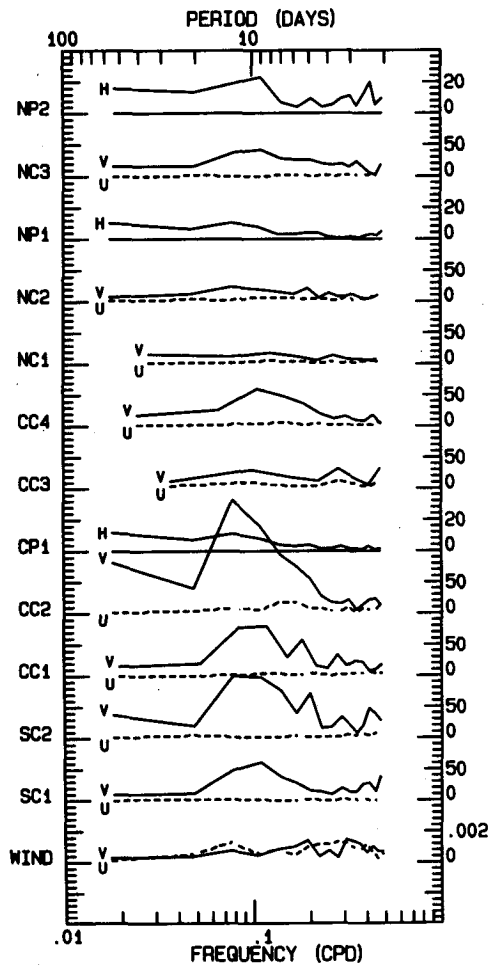


FIG. 3. Spectral estimates in energy-preserving form of sea level (H), alongshore (V) and across-shelf (U) components of current and wind stress within the study region. Units are cm^2 , $(\text{cm s}^{-1})^2$ and $(\text{N m}^{-2})^2$, respectively. Sequential block averaging over five adjacent spectral estimates has been performed, giving 10 d.f. for each point plotted.

Cape (tip of FI) and Pine Island (440 km alongshore) show that, during our observation period, the wave-number of the wind stress is in the range $-2 \times 10^{-6} \text{ m}^{-1} < k_0 < 1 \times 10^{-6} \text{ m}^{-1}$, for frequencies less than 0.2 cpd where significant coherence is seen. This corresponds to wavelengths always in excess of 3000 km and phase speeds greater than 8 m s^{-1} . The average value over the whole time period (180 days) is $k_0 = -4 \times 10^{-7} \text{ m}^{-1}$, corresponding to a wavelength of $\sim -16000 \text{ km}$ resolved in the northward alongshore direction and hence an apparently southward alongshore phase speed. (Hereafter, we will use simply "northward" to mean northwestward, i.e., in the equatorward alongshore direction.)

3. Barotropic wind-driven theory—prediction and comparison with data

In this section the observations are compared with a barotropic theory of the wind-driven response of the

ocean. The comparison is made for the northern end of the study region where the theoretical response is largest.

The water column was observed to be mostly well mixed over the shelf proper and the appropriate momentum equations in their barotropic form are

$$\frac{\partial u}{\partial t} - fv + g \frac{\partial \zeta}{\partial x} - \frac{\tau_w^x}{\rho h} + \frac{ru}{h} + u \frac{\partial u}{\partial x} + v \frac{\partial u}{\partial y} = 0 \quad (1)$$

$$\frac{\partial v}{\partial t} + fu + g \frac{\partial \zeta}{\partial y} - \frac{\tau_w^y}{\rho h} + \frac{rv}{h} + u \frac{\partial v}{\partial x} + v \frac{\partial v}{\partial y} = 0. \quad (2)$$

We have chosen axes x offshore and y alongshore with corresponding velocity components u and v , respectively. The Coriolis parameter is f , h is the depth, r a bottom friction parameter ($=5 \times 10^{-4} \text{ m s}^{-1}$ with a linear bottom friction law), ζ the surface elevation, and τ_w^x and τ_w^y are the across-shelf and alongshore components of the wind stress, respectively. The individual terms in (1) and (2) can be estimated from the data. This exercise is helpful in deciding which terms can be safely ignored in order to solve the equations. The terms may also be summed to check that they add to zero. Figures 4a and 4b show estimated magnitudes of the terms comprising (1) and (2). Finite difference methods are used to evaluate the gradients $\partial \zeta / \partial x$ and $\partial \zeta / \partial y$ from the three pressure gauges. These quantities are assumed to average to zero over the six-month deployment time. The velocity components u and v are those recorded by the coastal meter on the northern line, and the velocity gradients are estimated using adjacent current meters. Time derivatives are found from a second-order difference scheme which resolves motions of periods greater than four days.

Figures 4a and 4b show that the nonlinear terms may be safely ignored in both momentum equations and that the across-shelf acceleration, wind stress and bottom friction may also be ignored, greatly simplifying (1) and (2). Figure 4a shows that the dominant across-shelf momentum terms are, as anticipated, the geostrophic balance between alongshore current and across-shelf pressure gradient. The fact that the fluctuations of these quantities very nearly balance suggests that our two pressure gauges were sufficient to measure the pressure gradient across the entire shelf width, i.e., that this quantity is monotonic across the shelf. However, the long term trend in the momentum imbalance is a puzzling feature. It is due to the observed reduction in the coastal sea level that occurred while the outer shelf sea level remained constant. No such trend was recorded in the alongshore current and hence an apparent momentum imbalance exists. Temperature follows a similar trend but steric anomaly cannot account for either the sign or the magnitude of the sea level trend. Figure 4b shows that many terms are important in the alongshore momentum balance but that they have not been estimated accurately, and hence the apparent imbalance. Note that wind forcing is approximately balanced by bottom friction.

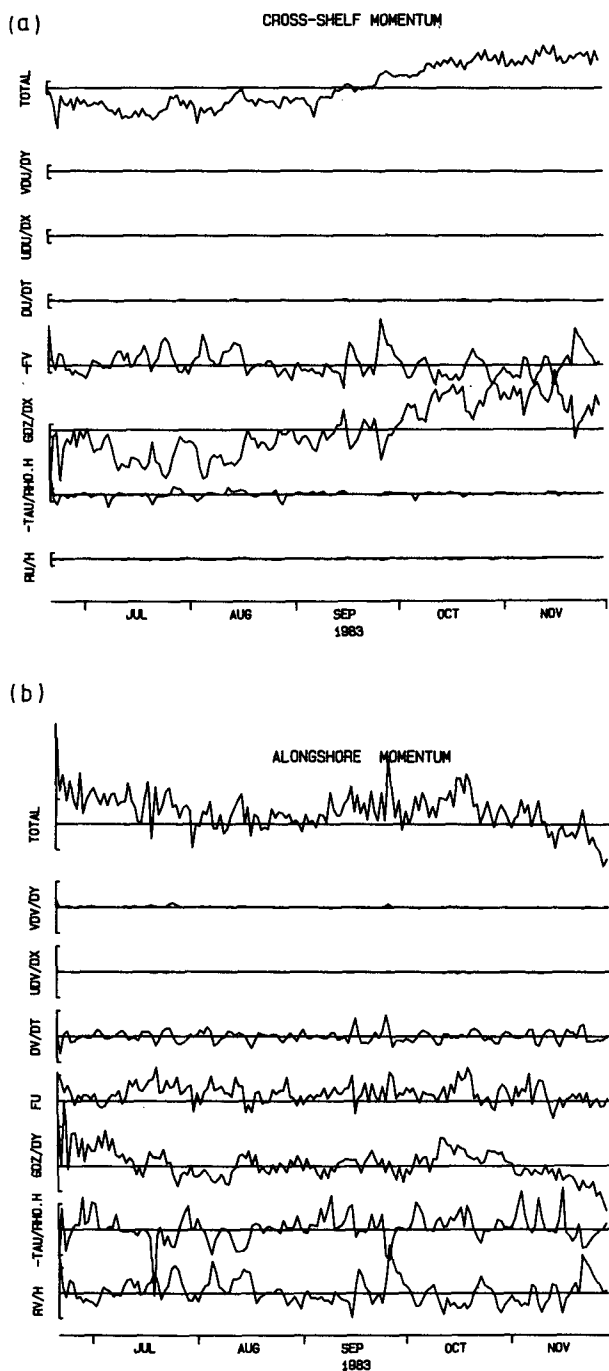


FIG. 4. (a) Cross-shelf and (b) alongshore momentum terms estimated from finite differences of adjacent daily datasets centered at NC3. The totals would be zero if momentum balance were observed. Tics on the vertical axes correspond to $3 \times 10^{-6} \text{ m s}^{-2}$.

To test the applicability of barotropic wind-forced shelf wave theory, the theory of Middleton and Cunningham (1984), which predicts wind-driven continental shelf waves from a geographical origin on a shelf of constant depth h adjacent to a deep ocean of depth h_0 , was chosen. While this theory was originally applied to explain wind-driven currents north of the Capricorn

Channel, it should also apply in the region north of FI. Subject to assumptions of nondivergent flow, a shelf width L which is narrow compared to the forcing scale, and oscillation frequencies much less than inertial, the simplified equations of motion are

$$fv = g \frac{\partial \zeta}{\partial x}, \tag{3}$$

$$\frac{\partial v}{\partial t} + fu = -g \frac{\partial \zeta}{\partial y} + \frac{\tau_w^y}{\rho h} - \frac{rv}{h}, \tag{4}$$

$$\frac{\partial}{\partial x}(hu) + \frac{\partial}{\partial y}(hv) = 0. \tag{5}$$

Defining a streamfunction ψ such that $u = -h^{-1}\partial\psi/\partial y$ and $v = h^{-1}\partial\psi/\partial x$ and noting the problem to be separable such that $\psi(x, y, t) = f(x)\phi(y, t)$, Middleton and Cunningham show that $f(x) = x, 0 < x < L$ for a step-shaped shelf, while the alongshore structure for a wind stress of form $\tau_0 \cos(k_0 y - \omega t)$ satisfies

$$\phi = \phi_0 \left[\cos\left(k_0 y - \omega t + \frac{\pi}{2} - \delta\right) - e^{-\gamma y} \cos\left(\frac{\omega y}{c} - \omega t + \frac{\pi}{2} - \delta\right) \right] \tag{6}$$

where

$$\phi_0 = \frac{\tau_0}{\rho c [\gamma^2 + (k_0 - \omega/c)^2]^{1/2}}, \tag{7}$$

$$\gamma = \frac{r}{ch}, \quad \tan \delta = \frac{\gamma}{(\omega/c - k_0)},$$

$$c = fL(1 - h/h_0). \tag{8}, (9), (10)$$

The solution represents the sum of a forced wave traveling at the speed of forcing (ω/k_0) and a free wave traveling with phase speed c . The free wave is damped by friction, and its amplitude decreases exponentially with distance from the origin (FI). The two cancel exactly at the origin so that the total response increases linearly (at first) with distance from the origin. Note that the response is much enhanced when the free wavenumber ($k = \omega/c = 1.5 \times 10^{-6} \text{ m}^{-1}$ at 0.10 cpd) is close to the wavenumber of the forcing k_0 , making a calculation of the response function sensitive to this measurement. This situation, however, does not arise in the present case because $k \sim -k_0$.

We compare theory with observation by calculating the complex velocity

$$w = u + iv \tag{11}$$

using both theoretical and observational approaches and then calculate the anticlockwise $H_A(\omega)$ (positive frequency) and clockwise $H_C(\omega)$ (negative frequency) response functions. From the above theory we calculate

$$H_C(\omega) = \frac{w_C(\omega)}{\tau_C(\omega)}, \quad H_A(\omega) = \frac{w_A(\omega)}{\tau_A(\omega)} \tag{12}$$

while the Fourier coefficients W_c and T_c evaluated from the data at frequency ω yield the observed estimates

$$H_c(\omega) = \frac{\overline{T_c^* W_c}}{\overline{T_c^* T_c}}, \quad H_A(\omega) = \frac{\overline{T_A^* W_A}}{\overline{T_A^* T_A}}. \quad (13)$$

Here the overbars denote band averaging in the frequency domain.

Figure 5 shows the predicted and observed anticlockwise rotary response function for the currents recorded by the coastal meter of the northern line. (The clockwise rotary response function is not shown here because much less coherence between wind and current is observed.) For the theoretical prediction we have chosen $L = 80$ km, $r = 5 \times 10^{-4}$ m s $^{-1}$, $h = 40$ m, $h_0 = 440$ m and allowed for an increase in the free-wave phase speed c by the presence of the outer reefs as predicted by Middleton (1983). The phase lag is about twice the predicted value at all frequencies but the gain agrees fairly well with theory. There is a significant peak, however, in the gain at 0.11 cpd, which is not predicted by theory. This signal is even greater at all other mooring sites, even though their predicted

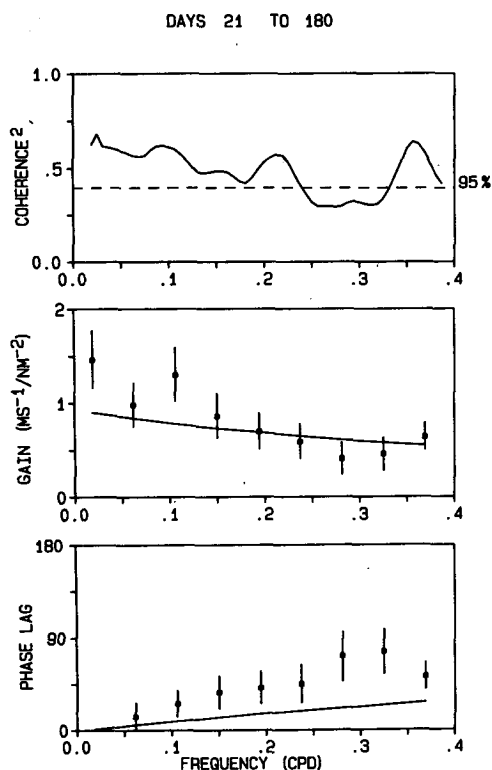


FIG. 5. Coherence squared and the gain and phase of the transfer function between the anticlockwise rotary components of wind stress and current at NC3. Phase lags are positive when the current lags the wind. For gain and phase the solid line represents the predicted transfer function and the squares represent estimates from the data. Error estimates (68%) of observed gain and phase, determined from coherence (Bendat and Piersol, 1980) are shown for each square plotted. Values are separated on the frequency axis by the half-width of the smoothing (7 Fourier coefficients). Day 21 is 21 June 1983.

gains are less. The lack of a good agreement between observed and predicted response at other locations within the study region is most likely due to the difficulty in separating the locally forced component of the current from the remotely forced component, which in the model is assumed to be blocked by FI. Although Thomson and Middleton (1985) have developed a method for separating free and forced contributions to shelf waves for selected idealized cases, their method is not strictly applicable here since the source of variability originating south of FI cannot be identified. This difficulty can be illustrated by observing the response of the ocean to the wind stress on the continental slope at the central line where very little response is expected. Figures 6a, 6b and 6c compare the alongshore components of current and wind by showing the energy, coherence squared, and gain as functions of frequency for three subintervals of the data in the time domain. Figure 6a shows a situation of considerable energy transfer from wind to current at frequencies centered around 0.11 cpd, with a gain of 4 m s $^{-1}$ /N m $^{-2}$, a factor of three times greater than it is farther north. However, during the second subinterval (Fig. 6b) the ocean is apparently no longer responding even though the spectrum of the wind forcing has not changed appreciably. During the third subinterval (Fig. 6c) the peak in the current energy returns to a degree, but there is no significant coherence between the wind and the current as there is in Fig. 6a. Hence, the existence of another energy source is implied, and the coherence between wind and current during the first subinterval could be due to the coherence between the other energy source and the wind during that time interval only.

Cross-spectral analysis of the local wind with the wind recorded at Norah Head (1000 km to the south) reveals that the spatial coherence of the observed wind did reduce with time during the study period. This is probably due to the fact that the dominating weather systems are generally large during June and July but become more localized as summer approaches (October and November). Hence, the odd behavior of the wind-current transfer functions depicted in Fig. 6 is explained, provided the distant wind is an energy source of the observed currents.

4. Source of the variability on the upper continental slope

To check the hypothesis of energy propagation from farther south, time series of currents from the northernmost ACE mooring were obtained. This mooring was located near Evans Head (29°S), 440 km south of Fraser Island on the continental slope in 200 m of water. As discussed by Freeland et al. (1986) and Church et al. (1986a,b) there are very low frequency (~ 50 day period) alongshore current fluctuations, which are attributed to East Australian Current eddies. Superimposed on this signal, however, are fluctuations of period 6–10 days. Figure 7 shows a plot of the alongshore

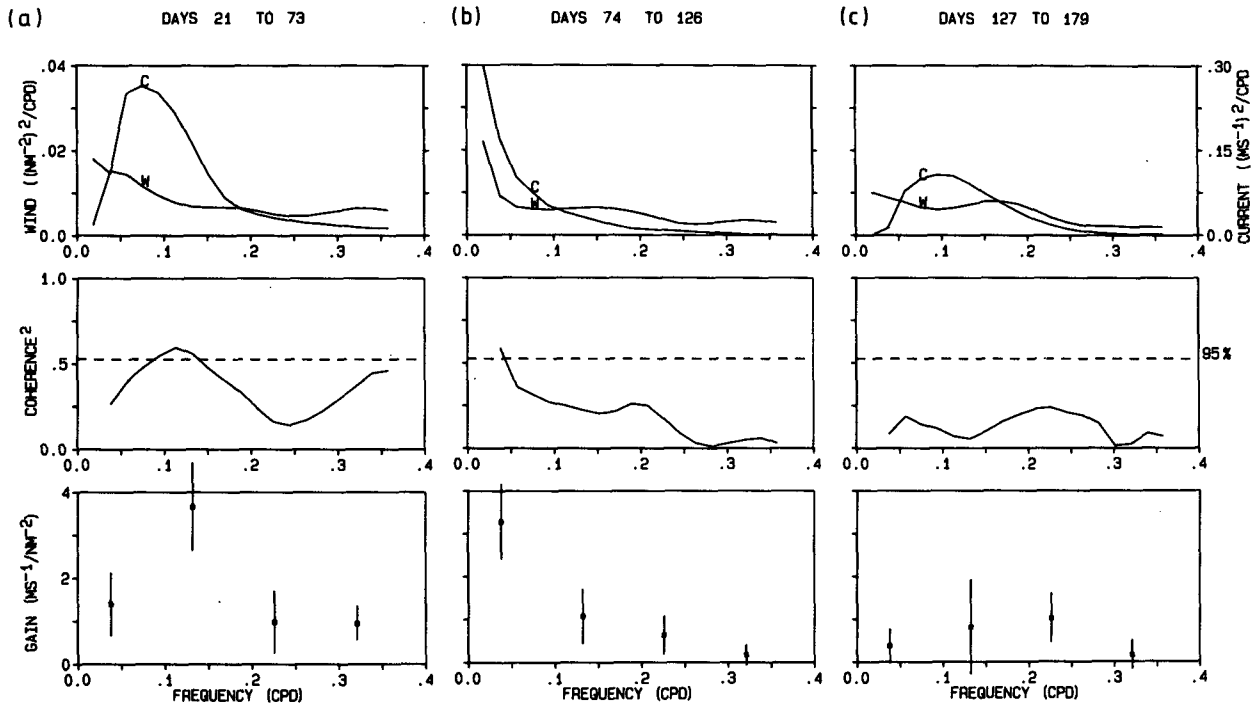


FIG. 6. Alongshore wind and current (meter CC2) autospectra, coherence squared, and gain for three consecutive subintervals of the data. Error bars are as for Fig. 5 but here the smoothing is over five Fourier coefficients.

velocity recorded by the Evans Head top meter for comparison with the alongshore velocity recorded by the southernmost top meter from north of FI. The fluctuations of 6–10 day period are visually correlated, with a northward propagation time of ~ 36 hours. Spectral analysis (not shown) confirms that the two time series have similar autospectra and that they are significantly coherent at the 95% confidence level for periods between 4 and 8 days. The phase difference at 0.12 cpd is $65 \pm 10^\circ$, representing 33 h, in agreement with the correlation estimate.

This evidence, in conjunction with the analysis of section 3, suggests that CTWs generated somewhere south of FI are the dominant force driving the currents within the study region north of FI. This result was unexpected. Our assumption that FI would serve as a

barrier to the northward energy flux of CTWs was based on the premise that the dominant mode south of FI would be a first-mode CTW that has strongest currents near the coast. This, indeed, was stated as one of the predictions for ACE by Clarke and Thompson (1984). However, a surprising result of ACE (Freeland et al., 1986, Church et al., 1986a,b) is that farther south on the New South Wales coast, much variability is seen on the continental slope, with the maximum near the shelf break instead of the coast. A portion of this variability is ascribed to eddy motions (and hence does not propagate north) but the second and third CTW modes are shown to be important, these having substantial northward energy flux on the continental slope. The data from Evans Head confirm that much variability is still evident on the upper continental slope 500 km north of the principal ACE region, but with only two meters at Evans Head it is not possible to perform a modal decomposition into CTW and eddy modes at this location. Hence it cannot be said which CTW modes are responsible for the northward propagation of current variability past FI.

Wang (1980) has examined numerically the interaction of the gravest mode continental shelf wave in a barotropic ocean with large topographic irregularities. He found that topographic features are important energy sinks of first-mode continental shelf waves because energy is transferred to motions with higher wavenumbers. The subsequent lower group velocities cause a water velocity amplification and greater dissipation. Davis (1981) has treated the problem analytically and

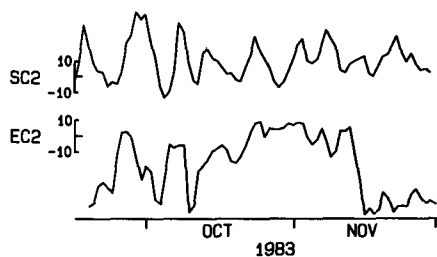


FIG. 7. Low-passed and daily-subsampled alongshore current from the northernmost ACE mooring at Evans Head (600 km south of the study region) for comparison with the alongshore current at the southernmost meter within the study region.

found that the principles of geometric optics apply. The wave is reflected at the coast, the promontory and the shelf break. Again, higher wavenumbers are excited. Unfortunately, neither author's work is directly applicable to the present case because both require exponential (or linear) shelf profiles, no stratification, and probably most importantly, irregularities smaller than FI. The present situation is further complicated by the presence of the Marion Plateau. Both authors' work, however, extrapolated to the present example, would probably call for total backscattering of the first-mode wave. There are, however, other possibilities. For example, the angle at which FI is inclined to the coast could result in the northward currents (from any mode) on the shelf being steered toward the shelf break, creating a region of strong cyclonic vorticity near the continental slope. The variation of this vorticity could then act as an energy source for the motions north of FI. ACE concluded that higher mode waves have significant energy farther south on the coast. If these are incident on FI then they may propagate past it more easily because they have considerable energy flux trapped over the continental slope.

Further observational and theoretical work is required for a complete understanding of CTW propagation past FI.

5. Propagation and structure of free baroclinic coastal-trapped waves within the study region

Having argued that CTWs are not completely blocked by FI we are faced with a difficult problem of modeling the currents observed within the study region north of FI.

The present case is made difficult by the need to know the wave field quite close to FI, the shoaling of the deep ocean in the vicinity of FI, the presence of intermittent reefs north of FI along the shelf break, and the sudden widening of the shelf at the Capricorn Channel 200 km north of FI. To solve a diffraction problem with all these factors considered is clearly beyond the scope of the present work. However, good results can be achieved with a surprisingly simple model, one in which FI and the reefs are ignored and no alongshore variations of the shelf profile allowed. This amounts to simply fitting the data to the CTW modes that are calculated for a long, straight coastline having the bathymetry and stratification representative of the central study region.

a. Fit of data to free CTW modes

The offshore structures of the alongshore velocity associated with the first three baroclinic CTW modes were calculated using a program written by K. Brink of Woods Hole. This program, which accepts arbitrary stratification and bathymetry and calculates all the allowed subinertial modal structures and dispersion re-

lations, has generously been made available to the oceanographic community and is discussed in Brink and Chapman (1985) and Brink (1982b).

The inviscid, unforced, linearized, long-wave equations are combined to form a single equation for the pressure field as a function of all independent variables: x , y , z and t . Assuming wavelike solutions in the alongshore direction, and with the depth profile $h(x)$ and stratification $N^2(z)$ independent of alongshore station y , application of the boundary conditions yields an eigenvalue problem with the pressure field being the eigenfunction of x and z . The eigenvalue determines the phase speed. Eigenfunctions and eigenvalues are found by resonance iteration, and the velocity field is calculated from the pressure field using the momentum equations.

Figure 8 shows the alongshore velocity fields of the first three modes as well as the positions of the current meters on the central line of moorings and the stratification (10 m bins) which was input to the program. Of the available density profiles, (Fig. 9) only three are from outside one baroclinic Rossby radius of deformation from the shelf break. These three were used as input to Brink's program since they are more likely to represent the time-independent stratification of the ocean.

We hypothesize that the observed motions can be expressed as a linear sum of the first two theoretical CTW modes. The third and higher modes are discussed later. The central line of current meters is used for the modal fit, which is performed using only three time series for each fit since the four current meters did not function concurrently. The Fourier transforms of the alongshore velocity time series at the three selected current meter sites yield, for the j th Fourier frequency, three observed complex velocity amplitudes which we write as the (complex) column matrix \mathbf{W} . The velocity fields of the theoretical CTW modes provide the (real valued) matrix \mathbf{V} , whose columns contain the relative amplitudes of alongshore velocity at the three current meter sites. We now have an equation for the j th set of complex modal coefficients \mathbf{a} :

$$\begin{bmatrix} V_{11} & V_{12} \\ V_{21} & V_{22} \\ V_{31} & V_{32} \end{bmatrix} \begin{bmatrix} a_{j1} \\ a_{j2} \end{bmatrix} = \begin{bmatrix} W_{j1} \\ W_{j2} \\ W_{j3} \end{bmatrix} - \begin{bmatrix} R_{j1} \\ R_{j2} \\ R_{j3} \end{bmatrix} \quad (14)$$

which may be solved in a least squares sense to minimize \mathbf{R} , the residuals. Equation 14 is solved for each resolvable Fourier frequency within the range 0–0.25 cpd (the CTW band). Strictly speaking, \mathbf{V} should be recalculated at each frequency but this is considered unnecessary since the modal structures do not vary appreciably over the frequency range of interest. Also note that \mathbf{V} is real valued because in this frictionless calculation of the CTW modes there are no across-shelf phase differences (Brink, 1982a).

The solution matrix \mathbf{a} contains the "best fit" of the two CTW modes to the observed currents. By back-

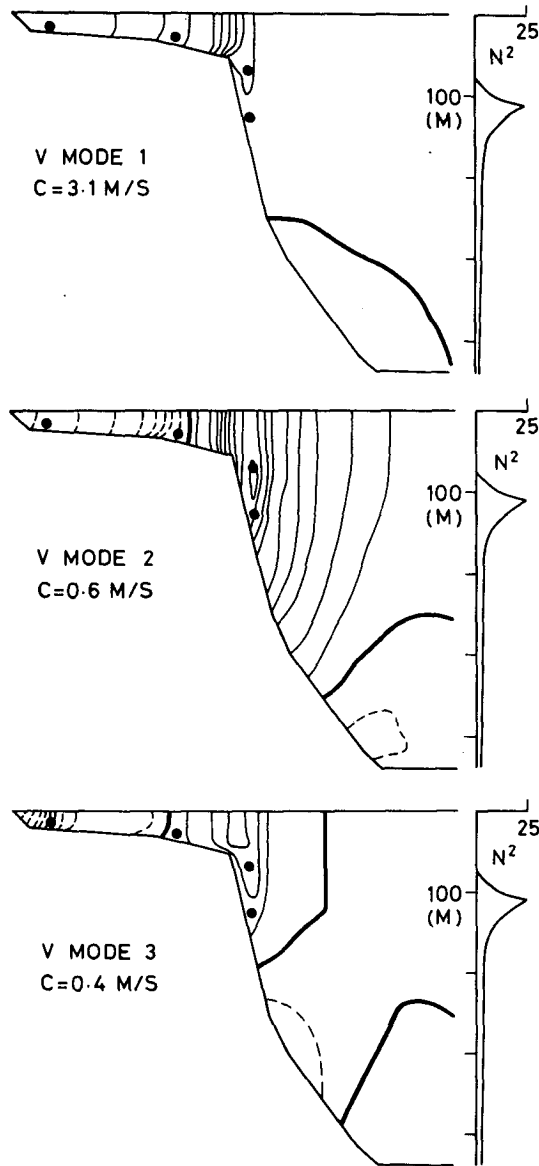


FIG. 8. Contour diagrams of the alongshore velocity amplitudes associated with the first three theoretical CTW modes for the shelf profile and stratification of the central study region. Velocity values are scaled relative to a maximum of ten contour intervals. The nodal lines are drawn heavily, negative velocities being dashed and circles indicating the positions of current meters. The low-frequency phase speeds and the N^2 profile used (units are 10^{-5} s^{-2}) are shown for each mode.

substitution of \mathbf{a} into (14) with $\mathbf{R} = \mathbf{0}$ and by taking the inverse Fourier transforms, three time series are produced. These are the individual "fits" at each current meter site to the time series data and are shown for comparison with the observed data in Fig. 10. It is clear that the majority of the observed variance has been ascribed to the two CTW modes. Also shown are the individual contributions of each mode to the total current at each location. At CC1 (and CC2, not shown) almost all the observed variance is ascribed to mode

2. At CC3, however, near the second mode's node, the variance is mostly due to mode 1. This possibly explains the considerable difference between the recorded currents at CC3 and at CC1 and CC2. The current meter at CC3 was thought to have malfunctioned for the entire deployment until its proximity to the first node of the higher modes was appreciated. Near the coast, at CC4, the two modes are added in near-antiphase to produce the fairly small observed current.

b. Validation of modal fit

A set of observations can always be expressed as a linear combination of eigenfunctions. To argue that the appropriate set of eigenfunctions has been used, some sort of predictive power must be demonstrated. A predicted velocity time series may be produced for an arbitrary location removed by Δy in the alongshore direction by calculating, for all appropriate j ,

$$W_j = \sum_{m=1,2} V_m a_{jm} \exp(ik_{jm}\Delta y) \quad (15)$$

where W_j is the j th Fourier component. The inverse Fourier transform then yields the time series. The row matrix \mathbf{V} contains the velocity amplitudes of the theoretical modes at the selected location in the x, z plane while \mathbf{k} contains the wavenumbers of the theoretical modes at the Fourier frequencies. The wavenumbers are evaluated for each mode and for each frequency using the dispersion relations calculated by Brink's program. Similarly, time series of the other dynamic variables u (cross-shelf velocity), w (vertical velocity) and p (pressure) may be produced since their relationship to v is given by CTW theory. However, these

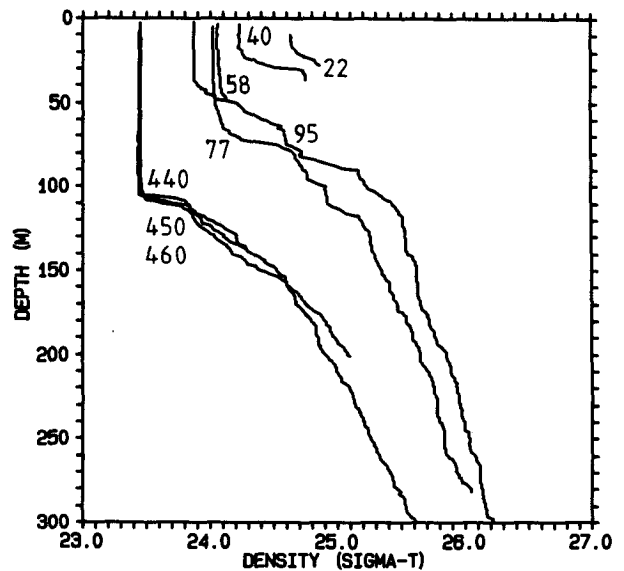


FIG. 9. Density profiles from a CTD transect along the central line performed on the deployment cruise. Traces are labeled with the distance (km) from the coast. The three most seaward profiles were used for the stratification (Fig. 8) input to Brink's CTW program.

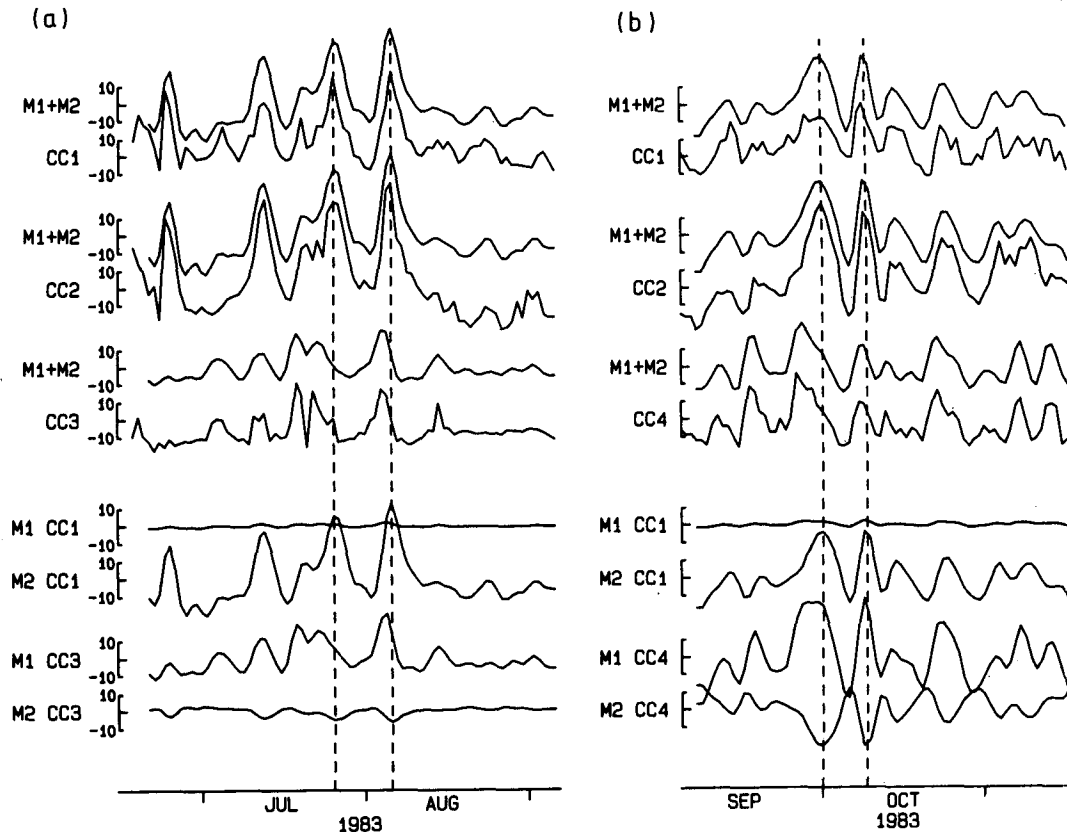


FIG. 10. Comparisons of observed alongshore velocities with modal fits using the first two CTW modes. Meters CC3 and CC4 did not function concurrently for long so the decomposition was performed using (a) CC3 and (b) CC4. In each case the upper three paired traces compare data with the combined mode-1 plus mode-2 (M1 + M2) fit, while the lower two paired traces simply show the individual contributions from modes 1 and 2, separately. Time marker lines (dashed) are centered on current maxima.

quantities are much harder than v to measure directly over the continental slope because they are much smaller. Temperature may easily be measured but is more difficult to hindcast because it is a nonlinear function of the vertical displacement. Its amplitude is hindcast by solving

$$p = g \int_{z'}^{z'+\zeta} [\rho(z-\zeta) - \rho(z)] dz \quad (16)$$

numerically for ζ , an estimate of the vertical isotherm displacement and then finding $t = t(z' + \zeta) - t(z')$. Here, p is the hindcast pressure amplitude at the selected location while $\rho(z)$ and $t(z)$ are the observed density and temperature profiles. The modal contributions are summed analogously to (15).

With $\Delta y = 0$ the "missing data" from the fourth meter can be hindcast from the three functioning meters on the central line. Realistic time series result, but are not shown because no comparison with observation is possible. With $\Delta y = -34$ km time series for the southern mooring can be hindcast. Figure 11 shows three comparisons of hindcast time series with observed time series. Alongshore velocity is shown for SC1 and

SC2 while temperature is also shown for SC1, the deeper meter which experienced negligible mooring layover. It is clear that temperature fluctuations over the continental slope are well predicted by explaining the alongshore current in terms of CTW modes. The important feature of the good agreement between the observed and hindcast velocity traces is that the observed one-day lead of the southern time series over the central time series is also well predicted. This large observed time difference initially aroused suspicions that the data were not correctly oriented in time. Cross-spectra at high frequencies confirmed their correct orientation and calculation of the free baroclinic CTW modes provided the explanation. Time marker lines are drawn on Figs. 10 and 11 at the times of maximum current seen at the central line so that this time difference is apparent. This feature is also demonstrated by Fig. 12 which shows, as a function of frequency, the observed phase difference between the alongshore current at CC2 and SC2 for comparison with the prediction of the modal fit. Also shown are the phase lags that would be seen if the propagating signal were purely mode 1, 2 or 3. At most of the resolvable frequencies, the observed phase lag agrees with the fit to the first

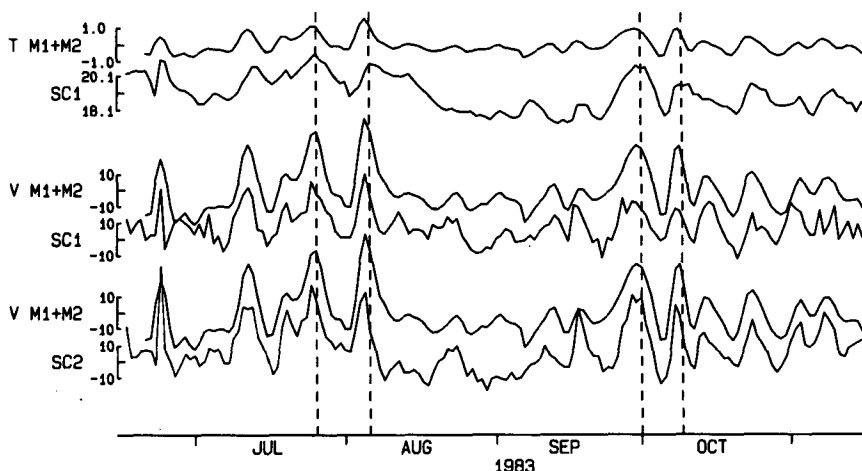


FIG. 11. Comparisons of time series of alongshore velocity and temperature recorded by the two meters of the southern mooring with the hindcasts of the modal fit depicted in Fig. 10. The observed and hindcast current maxima precede the time marker lines (repeated from Fig. 10) by the same amount, indicating the time lags are well predicted by the modal fit.

and second modes, being predominantly second mode at this offshore location. However, at 0.11 cpd where the coherence is actually greatest between the two time series (error bar smallest), it seems that the third mode's phase lag is more appropriate. Similar results (not shown) are achieved for both current and temperature at CC1 and SC1.

The whole procedure as outlined may be repeated using the third instead of the second theoretical CTW mode. Hindcast time series (not shown) are very similar to those shown in Figs. 10 and 11. The predicted phase lags (not shown) between CC2 and SC2 are very close to those of the third mode, improving the agreement with observation at 0.11 cpd (perhaps the most important frequency) at the expense of other frequencies. The relative amplitudes of alongshore velocity at 60

and 130 m depth are fitted more successfully to the third mode, at the expense of the near-coastal amplitude. Observed temperature amplitudes are also more easily accounted for by fitting currents to the third mode.

We cannot, however, formally distinguish the second and third mode contributions to the observed data by their offshore structures. To do this would require a denser instrument array extending to greater depth. With the available data and all three modes used, the solution to (14) for the modal coefficients is unstable to small perturbations. Theoretical and observed temperature amplitudes may also be used for the modal fit but this does not successfully distinguish the second and third modes. It is possible that the fourth and higher modes are also important, but this possibility cannot be examined with the available dataset.

The modal decomposition and the comparison of hindcast time series with observations discussed above indicate that higher (i.e., the second and/or third) mode CTWs are important for the transmission of energy into and through the southern half of the study region. However, the hindcast predictions for the northern line are not quite so satisfactory. As mentioned above, at CC4 the first and second mode are added in near-antiphase (Fig. 10a) to produce the small observed current, and closer to FI they add even closer to antiphase. Hence at NC3, the northern coastal meter, very strong currents are predicted by the modal fit. That these are not seen suggests severe attenuation of the higher modes. The observed phase lag between CC4 and NC3 is small, indicating that the slow higher modes do not propagate between the central and northern lines along the coastal boundary. Nor is there evidence of the higher modes in the data from NC1 or NC2 farther offshore, although the possibility exists that these meters were situated close to the nodes of those modes.

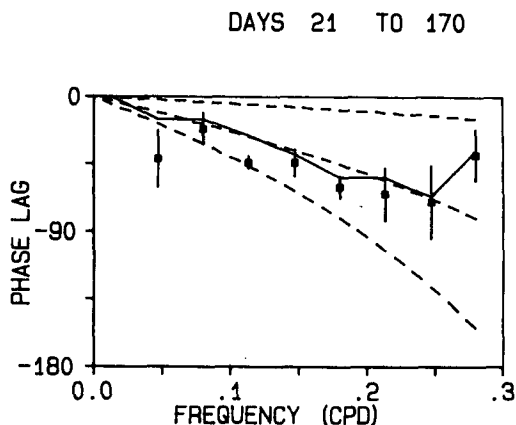


FIG. 12. Hindcast (solid line) and observed (squares) phase differences between the alongshore currents at SC2 and CC2. Error estimates of observed phase lags are as for Fig. 5. The three dashed lines, indicating mode 1, 2 and 3 phase lags are effectively dispersion curves where the phase lag is given by ky and $y = 34$ km.

The pressure gauges have not detected the higher modes either but they cannot be expected to do so. As Hsieh (1982) has pointed out, the first mode dominates the pressure data due to its much enhanced expression. The maximum sea level/maximum current amplitude ratio reduces with increasing mode number. In the present example, these ratios are 0.27 m/m s^{-1} for the first mode and 0.05 m/m s^{-1} for the third, so the pressure signal from the third mode will be indistinguishable from the noise in the data.

There are several reasons why the higher modes should be less evident at the northern line: (i) their much slower phase speeds give them much shorter alongshore decay lengths, (ii) a long, thin barrier along the shelf break (such as the outer reefs) has been shown by Hsieh and Buchwald (1985) to transfer energy from higher modes to the Kelvin mode on the shelf and to the first mode on the slope, and (iii) the higher modes are probably more strongly affected by the shoaling of the Marion Plateau which rises from 520 to 440 to 300 m off the southern, central and northern lines of meters. Davis (1983) and Wang (1980) have discussed how CTWs adjust to changing bathymetry, but neither study is directly applicable to the present case. A shoaling ocean could lead to water velocity amplification, as is observed between the southern and central lines, due to the energy flux being concentrated into less depth. Water velocities approach the phase speeds of the higher modes at the central line, implying that further shoaling of the Marion Plateau would lead to nonlinear interactions becoming increasingly important; however, the consequences of this are beyond the scope of the present work.

c. Dynamics of CTW modes

A brief description will now be given of the dynamics of the theoretical CTW modes calculated for the study region. As an aid to visualizing these waves, Fig. 13 shows perspective views of the first two modes' sea surface and thermocline expressions with the accompanying currents also indicated. These diagrams are indicative only of the salient features of the modal structures. The first mode's structure is the familiar simple system which has been discussed by many authors. The higher modes' structures are very dependent on stratification, shelf profile, and Coriolis parameter and have been discussed in detail by Huthnance (1978), Wang and Mooers (1976) and Brink (1982b).

In the present case, the second and third modes have similar structures over the continental slope to the first and second baroclinic modes calculated for the same continental slope with no shelf region adjoining. This is significant because it allows efficient coupling with the modes calculated for the continental slope adjacent to FI. The third mode resembles the second over the shelf and in the upper ocean (which is why we cannot distinguish them) but features an additional surface at greater depth moving in antiphase with the one illustrated. The second (third) CTW mode consists basically

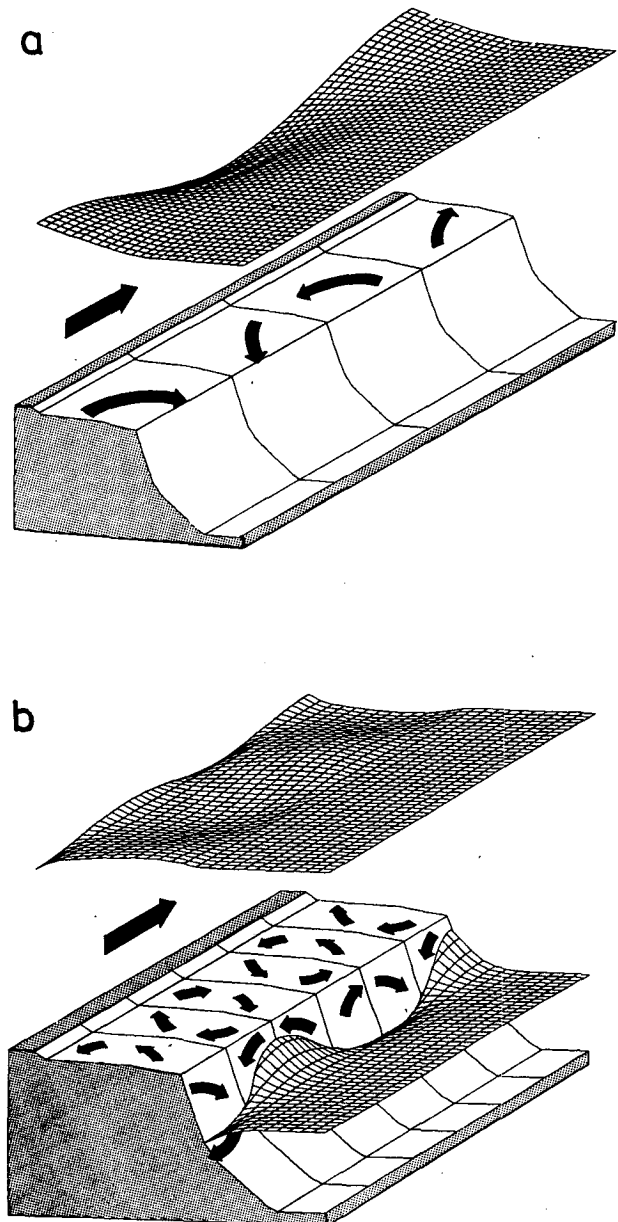


FIG. 13. Salient features of the CTW modes calculated for the study region. The first mode (a) is shown compressed in the alongshore direction by a factor of ~ 4 . The sea surface displacements are greatly exaggerated in both illustrations and the surface lifted to reveal the associated currents. Isotherm motion is less exaggerated. The second- and third-mode structures in the upper ocean are similar and are both adequately depicted by (b), although the third mode would have additional complexity at greater depth.

of two (three) counter-rotating gyres, one on the shelf and one (two) bottom-trapped against the continental slope. On the shelf the flow is approximately geostrophic where velocity amplitudes are high, the pressure gradients being provided by sea surface slopes. This applies at midshelf for the across-shelf currents and at the coast and outer shelf for the alongshore currents. Where velocity amplitudes are low the pressure

gradients are balanced by accelerations, e.g., at midshelf where the alongshore current has a node the across-shelf acceleration balances the across-shelf pressure gradient. The motion on the continental slope may be envisaged as gyres whose axes are normal to the continental slope, pressure gradients being produced by large isopycnal displacements. The density contribution to the total potential energy is 80 (20) times that of the free surface and the alongshore current contribution to the kinetic energy is 30 (5) times that of the across-shelf current. Kinetic energy exceeds potential energy by a factor of 28 (25). This latter ratio has been used to parameterize wave type (1 \equiv baroclinic Kelvin wave, ∞ \equiv barotropic shelf wave) but Brink (1982b) points out that this diagnostic parameter is not very discriminating for short, bottom-trapped waves.

6. Discussion

Observations of sea level, current and temperature in a study region north of Fraser Island (FI) on the east coast of Australia show substantial energy at subinertial frequencies. Near-coastal currents within the study region are reasonably well predicted by a simple barotropic theory of wind-driven circulation, which assumes that FI acts as a geographical origin for first-mode continental shelf waves. On the continental slope, however, subinertial frequency currents have energy far in excess of that predicted by the simple wind-driven circulation model. Comparison with data from farther south of FI suggests that the relatively high current variability on the slope occurs as a result of the propagation of coastal-trapped waves along the continental slope past FI and into the study region.

To test the applicability of CTW theory to the observed currents within the study region, the across-shelf structure of the alongshore current was decomposed into CTW modes at one instrument line. Using predicted phase speeds the modes were then "propagated" to a second instrument line and the current time series resynthesized. Close resemblance of predicted and observed alongshore currents at the second line indicates that linear CTW theory successfully explains propagation of variability within the study region.

The modal decomposition shows that the second and/or third CTW modes, having substantial energy content on the slope, carry the majority of energy with the dominant signal having a period of ~ 9 days, an alongshore current amplitude on the upper slope of ~ 20 cm s^{-1} , and a northward phase speed of ~ 0.4 m s^{-1} . Propagating with the current fluctuations are temperature fluctuations of $\sim 1.0^\circ C$, suggesting vertical thermocline excursions of ~ 30 m.

The factors that point to the existence of the second- or third-mode CTW are as follows:

- (i) The relative amplitudes of alongshore velocity recorded by the four current meters on the central line resemble a superposition of the first and higher modes, with the latter being more important.
- (ii) Both the alongshore velocity and temperature signals observed on the continental slope propagate at phase speeds near those of the second and third modes.
- (iii) The phase and amplitude of the temperature fluctuations recorded by the four current meters on the continental slope are well predicted by the third mode, and to a lesser degree by the second.
- (iv) The second and third modes produce little net alongshore fluid transport at any instant on the shelf, and hence the existence of Fraser Island is not too restrictive a southern boundary condition.
- (v) Considerable energy flux is to be expected on the continental slope, which is not obstructed by Fraser Island, and hence there exists an avenue for the input of energy into the second and third modes.
- (vi) Wang (1980) showed that, in a barotropic ocean, energy in the form of a gravest mode shelf wave can be forward and backscattered by an obstacle into short modes that decay in the vicinity of the scatterer. His predictions are plausibly extrapolated to the present case of a stratified ocean with first and higher modes incident on a very large obstacle.

We now turn our attention to the possible biological significance of CTWs on Australia's east coast. The temperature records from the pressure gauge on Lady Musgrave Island at the shelf break on the central line and, to a lesser extent, those from the current meter 10 km inshore suggest that the thermocline motion seen on the continental slope is of sufficient amplitude to result in the upwelling of cold water, presumably nutrient rich, onto the shelf. CTD casts (Fig. 9) taken on the continental slope show large isopycnal displacements, while those over the shelf show a pool of dense water in the lagoon, supporting this hypothesis.

Hatcher and Larkum (1983) have determined experimentally that nitrogen availability is a major limiting factor to biomass production on One Tree reef, situated on the outer shelf between the central and northern lines of the present study region. Production in the lagoon is greatest during winter and spring, when ambient nitrogen levels are highest and temperatures are lowest, indicating that growth is not limited by low temperatures. Experimental enrichment of nitrogen confirms its importance. Hence it appears plausible that nutrient upwelling by CTWs is important to the sustainment of the considerable biological activity within the study region.

CTWs may also have geological relevance. It seems that the dune islands off Queensland are the result of arrested northward sediment transport from the southeast coast of Australia. The model of Roy and Thom (1981) envisages this transport to be due to the mean alongshore drift due to the predominantly northwestward swells from the Tasman Sea. As the coastline curves around from northeasterly to northwesterly at lower latitudes the reduced wave energy on the shelf supposedly results in net deposition.

We now speculate that if CTWs were to cause a net

alongshore sediment transport then this transport may well be arrested when the CTWs encounter the Marion Plateau. This provides an alternative or supplementary explanation for the formation of FI (the Great Sandy Island) adjacent to the Marion Plateau.

Acknowledgments. This work was supported by Australian Marine Sciences and Technologies Grants Scheme, Grant 82/1137. David Griffin is grateful to the Postgraduate Research Awards Scheme for a scholarship during his Ph.D. candidature. We would like to thank Greg Nippard for his field work and electronics expertise and Rhona Metzker for typing the manuscript. We are especially indebted to the CSIRO for time on RV *Sprightly*, to the ACE team for Evans Head current meter data, and to Ken Brink for the use of his coastal-trapped wave program.

REFERENCES

- Allen, J. S., 1980: Models of wind-driven currents on the continental shelf. *Annual Reviews in Fluid Mechanics*, Vol. 12, Annual Reviews, 389-433.
- Bendat, J. S., and A. G. Piersol, 1980: *Engineering Applications of Correlation and Spectral Analysis*, Wiley & Sons, 278-280.
- Brenner, N. M., 1967: Three Fortran programs that perform the Cooley-Tukey Fourier transform. Tech. Note 1967-2, Lincoln Laboratory, M.I.T., 29 pp.
- Brink, K. H., 1982a: The effect of bottom friction on low-frequency coastal trapped waves. *J. Phys. Oceanogr.*, **12**, 127-133.
- , 1982b: A comparison of long coastal trapped wave theory with observations off Peru. *J. Phys. Oceanogr.*, **12**, 897-913.
- , and D. C. Chapman, 1985: Programs for computing properties of coastal-trapped waves and wind-driven motions over the continental shelf and slope. Woods Hole Oceanographic Inst. Tech. Rep. WHOI-85-17, 98 pp.
- Church, J. A., H. J. Freeland and R. L. Smith, 1986a: Coastal trapped waves on the east Australian continental shelf. Part I: Propagation of modes. *J. Phys. Oceanogr.*, **16** (in press).
- , N. J. White, A. J. Clarke, H. J. Freeland and R. L. Smith, 1986b: Coastal trapped waves on the east Australian continental shelf. Part II: Model verification. *J. Phys. Oceanogr.*, **16** (in press).
- Clarke, A. J., and R.O.R.Y. Thompson, 1984: Large scale wind-driven ocean response in the Australian coastal experiment region. *J. Phys. Oceanogr.*, **14**, 338-352.
- Davis, A. M. J., 1981: The scattering by a headland of the dominant continental shelf wave. *Phil. Trans. Roy. Soc. London*, **A303**, 383-431.
- , 1983: Shelf similar topographies for free continental shelf waves. *Geophys. Astrophys. Fluid Dyn.*, **23**, 321-331.
- Freeland, H. J., F. M. Boland, J. A. Church, A. J. Clarke, A. M. G. Forbes, A. Huyer, R. L. Smith, R. O. R. Y. Thompson and N. J. White, 1986: The Australian coastal experiment: a search for coastal-trapped waves. Submitted to *J. Phys. Oceanogr.*
- Hamon, B. V., 1962: The Spectrums of mean sea level at Sydney, Coff's Harbour and Lord Howe Island. *J. Geophys. Res.*, **67**, 5147-5155. (Correction, *J. Geophys. Res.*, **68**, p. 4635).
- , 1966: Continental shelf waves and the effects of atmospheric pressure and wind stress on sea level. *J. Geophys. Res.*, **71**, 2883-2893.
- Hatcher, B. G., and A. W. D. Larkum, 1983: An experimental analysis of factors controlling the standing crop of the epilithic algal community on a coral reef. *J. Exp. Mar. Biol. Ecol.*, **69**, 61-84.
- Hsieh, W. W., 1982: On the detection of continental shelf waves. *J. Phys. Oceanogr.*, **12**, 414-427.
- , and V. T. Buchwald, 1985: The scattering of a continental shelf wave by a long thin barrier lying parallel to the coast. *J. Phys. Oceanogr.*, **15**, 524-532.
- Huthnance, J. M., 1978: On coastal trapped waves: Analysis and numerical calculation by inverse iteration. *J. Phys. Oceanogr.*, **8**, 74-92.
- Middleton, J. H., 1983: Low frequency trapped waves on a wide reef-fringed continental shelf. *J. Phys. Oceanogr.*, **13**, 1371-1382.
- , and A. Cunningham, 1984: Wind-forced continental shelf waves from a geographical origin. *Contin. Shelf Res.*, **3**, 215-232.
- Mysak, L. A., 1980a: Recent advances in shelf wave dynamics. *Rev. Geophys. Space Phys.*, **18**, 211-241.
- , 1980b: Topographically trapped waves. *Annual Reviews in Fluid Mechanics*, Vol. 12, Annual Reviews, 45-76.
- Pierson, C. A., J. D. Schumacher and R. D. Muench, 1981: Effects of wave induced mooring noise on tidal and low frequency current observations. *Deep-Sea Res.*, **28**, 1223-1229.
- Roy, P. S., and B. G. Thom, 1981: Late Quaternary marine deposition in New South Wales and Southern Queensland—An evolutionary model. *J. Geol. Soc. Aust.*, **28**, 471-489.
- Thomson, R. E., and J. H. Middleton, 1985: On wavenumber estimates for forced continental shelf waves. *J. Phys. Oceanogr.*, **15**, 33-45.
- Walters, R. A., and C. Heston, 1982: Removing tidal period variations from time series data using low-pass digital filters. *J. Phys. Oceanogr.*, **12**, 112-115.
- Wang, D.-P., 1980: Diffraction of continental shelf waves by irregular alongshore geometry. *J. Phys. Oceanogr.*, **10**, 1187-1199.
- , and C. N. K. Mooers, 1976: Coastal trapped waves in a continuously stratified ocean. *J. Phys. Oceanogr.*, **6**, 853-863.
- Woodhead, P. M. J., 1970: Sea surface circulation in the southern region of the Great Barrier Reef, Spring 1966. *Aust. J. Mar. Freshwater Res.*, **21**, 89-102.
- Wu, J. W., 1982: Wind stress coefficients over sea surface from breeze to hurricane. *J. Geophys. Res.*, **87**, 9704-9706.